Solving the advection-diffusion equation on unstructured meshes with discontinuous/mixed finite elements and a local time stepping procedure

Charbel Pierre El Soueidy, Anis Younès, Philippe Ackerer

Solving the advection–diffusion equation on unstructured meshes with discontinuous/mixed finite elements and a local time stepping procedure

Ch. P. El Soueidy, A. Younes and P. Ackerer*, †

Laboratoire d'Hydrologie et de Géochimie de Strasbourg, Université de Strasbourg/EOST, CNRS 1 rue de Blessig, 67000 Strasbourg, France

Explicit schemes are known to provide less numerical diffusion in solving the advection–diffusion equation, especially for advection-dominated problems. Traditional explicit schemes use fixed time steps restricted by the global *CFL* condition in order to guarantee stability. This is known to slow down the computation especially for heterogeneous domains and/or unstructured meshes. To avoid this problem, local time stepping procedures where the time step is allowed to vary spatially in order to satisfy a local *CFL* condition have been developed.

In this paper, a local time stepping approach is used with a numerical model based on discontinuous Galerkin/mixed finite element methods to solve the advection–diffusion equation. The developments are detailed for general unstructured triangular meshes.

Numerical experiments are performed to show the efficiency of the numerical model for the simulation of (i) the transport of a solute on highly unstructured meshes and (ii) density-driven flow, where the velocity field changes at each time step.

The model gives stable results with significant reduction of the computational cost especially for the non-linear problem. Moreover, numerical diffusion is also reduced for highly advective problems.

KEY WORDS: discontinuous Galerkin finite elements; mixed finite elements; local time stepping; advection–diffusion equation; time splitting; density-driven flow

*Correspondence to: P. Ackerer, Laboratoire d'Hydrologie et de Géochimie de Strasbourg, Université de Strasbourg/ EOST, CNRS 1 rue de Blessig, 67000 Strasbourg, France.

†E-mail: ackerer@imfs.u-strasbg.fr

Contract/grant sponsor: ANDRA

1. INTRODUCTION

The most common mathematical model to simulate heat or mass transfer is an advection–diffusion-type partial differential equation, which has the following formulation:

$$L(C)=\frac{\partial C}{\partial t}+\nabla\cdot(\mathbf{V}C)-\nabla\cdot(\mathbf{D}\nabla C)=0,\quad \mathbf{x}\in\Omega,\ \ t\in[0,T] \tag{1}$$

where $C(\mathbf{x},t)$ [M/L^3] is the unknown concentration at location $\mathbf{x}$ and time t and $\mathbf{D}$ [L^2/T] is the diffusion tensor. In case of transport in porous media, this tensor is defined by

$$D_{ij}=(\alpha_T|\mathbf{V}|+D_{\mathrm{m}})\delta_{ij}+(\alpha_L-\alpha_T)\frac{v_i v_j}{|\mathbf{V}|},\quad i,j=1,\ldots,2 \tag{2}$$

$L(C)$ is the differential operator, $\mathbf{V}$ [L/T] is a given fluid velocity of components v_i, α_L and α_T [L] are the longitudinal and transverse dispersivities, δ_{ij} is the Kronecker delta function, and D_{m} [L^2/T] is the molecular diffusion coefficient. T is the end of the simulation time period starting at time zero.

Equation (1) is subject to the initial and boundary conditions

$$\begin{aligned} C(\mathbf{x},0)&=C_0(\mathbf{x}),\quad \mathbf{x}\in\Omega\\ C(\mathbf{x},t)&=g_1(\mathbf{x},t),\quad (\mathbf{x}\in\partial\Omega^1,t>0)\\ (-\mathbf{D}\nabla C)\cdot\boldsymbol{\eta}_\Omega&=g_2(\mathbf{x},t),\quad (\mathbf{x}\in\partial\Omega^2,t>0)\end{aligned} \tag{3}$$

where Ω is a bounded, polygonal open set of $\mathbb{R}^2$, $\partial\Omega^1$ and $\partial\Omega^2$ are partitions of the boundary $\partial\Omega$ of Ω corresponding to Dirichlet and Neumann boundary conditions, and $\boldsymbol{\eta}_\Omega$ is the unit outward normal to the boundary $\partial\Omega$.

Standard Eulerian numerical methods, such as finite elements or finite volumes, can be used to solve Equation (1). However, in many porous media applications, especially for small-scale simulations, the transport is advection-dominated and the differential equation becomes hyperbolic [1]. Hyperbolic equations have moving discontinuities or sharp fronts that classical methods fail to capture and give solutions with non-physical oscillations and/or numerical diffusion [2]. More accurate results can be obtained by refining both the spatial and temporal discretizations increasing the computational cost considerably.

On the other hand, the discontinuous Galerkin (DG) method has received more interest in the last two decades [3–5]. The flexibility of the DG method is its main advantage compared with other standard Euler schemes (finite volumes, finite elements), especially in handling complicated geometries, in defining strategies for grid refinement or coarsening, and/or in changing the degree of approximation from one element to the other. Moreover, the DG solution satisfies the mass conservation principle element by element.

Since the first DG method introduced in Reed and Hill [6], the methods have been developed for hyperbolic problems [7, 8] and for elliptic problems [9–13]. A unified analysis for many DG methods for elliptic problems is given in Arnold *et al.* [14].

When used for partial differential equations containing higher than first-order spatial derivatives, the DG methods have more degrees of freedom compared with the traditional finite element

methods. This is often considered as a drawback of the DG or the local discontinuous Galerkin (LDG) methods [15]. Moreover, the unknowns of the LDG method in any element depend, in general, on the neighbors of the element and the neighbors of the neighbors [4], which leads to a less sparse system matrix than with standard methods.

Contrarily to the DG methods for elliptic problems, the DG methods for hyperbolic systems have been proven to be clearly superior to the already existing finite element methods [14]. With DG, we obtain a high-resolution scheme for advection, which maintains the local conservation of finite volume methods but allows high-order approximations to enter through a variational formulation rather than by some hybridized difference or functional reconstruction [16].

Therefore, to solve the whole advection–diffusion equation, time splitting techniques are often applied to Equation (1). Advection and diffusion are then solved using different numerical techniques that are specifically suited to achieve high accuracy for each type of equation [17–19]. In the literature, several authors [3, 20] combined the DG method for advection with the mixed finite element method for diffusion. Indeed, the mixed finite element method is well suited for diffusion since it is locally conservative and can handle general irregular grids. This strategy will be adopted in this paper. The transport equation is solved with the explicit upwind DG method for advection combined with the implicit mixed finite element method for diffusion.

Traditional explicit models are often restricted by the global *CFL* condition in order to guarantee stability. This is known to slow down the computation especially for heterogeneous domains and/or unstructured meshes. To avoid this problem, a local time stepping procedure where the time step is allowed to vary spatially in order to satisfy a local *CFL* condition is used. In the literature, the local time stepping procedure is often combined with finite volume-type methods [21–26] and a very few papers extend the procedure to discontinuous finite elements [27–29]. The procedure was applied to the Euler equations in [27, 28] and to the Maxwell equations in [29].

In this study, the local time stepping procedure from [21] is coupled to the explicit/implicit DG/mixed methods to solve the advection–diffusion equation. It is shown that the procedure is not very difficult to implement and allows an important reduction of the computational cost without significant loss of accuracy.

In the first part of this paper, we present in detail the explicit DG method used to solve the hyperbolic part of the equation coupled with an implicit mixed finite element method used to solve the diffusive part of the equation. In the second part, the local time stepping is explained in detail for unstructured triangular meshes. The last part of the paper deals with numerical experiments performed to analyze the efficiency of the numerical model for the simulation of (i) the transport of a solute on highly unstructured meshes and (ii) a density-driven flow problem. The results are compared with the more traditional explicit/implicit approach described in [3]. Accurate results are obtained with a significant reduction of the computational cost. Moreover, the local time stepping procedure provides less numerical diffusion than the standard explicit scheme for high-advective transport problems.

2. NUMERICAL RESOLUTION OF THE ADVECTION–DIFFUSION EQUATION

2.1. The time splitting procedure

Operator and time splitting (e.g. [30]) offer the possibility to adopt an accurate numerical technique for each kind of partial differential equation. Therefore, the transport equation (1) is solved as

follows:

- First, advected concentrations C^{adv} are obtained by the resolution of the advection equation

$$\frac{\partial C}{\partial t} + \nabla \cdot (\mathbf{V} C^n) = 0 \tag{4}$$

- Then, obtained results are used as initial concentrations for the resolution of the diffusion equation

$$\frac{\partial C}{\partial t} = \nabla \cdot (\mathbf{D} \nabla C^{n+1}) \tag{5}$$

The time splitting technique allows the resolution of the separate partial differential equations (4) and (5) with different time steps. We define Δt_{A} and Δt_{D}, respectively, as the advective and diffusive time steps that are used for all cells. Since we use an implicit scheme for the diffusion equation, there is no stability restriction and large time steps can be used for the resolution of Equation (5). Therefore, we can assume the existence of an integer $M \geqslant 1$ that satisfies $\Delta t_{\text{D}} = M \Delta t_{\text{A}}$.

Let $\varepsilon_{\text{A}}^{\Delta t_{\text{A}}}(C)$ denote the DG operator (including the slope limiting process) that advances the pure hyperbolic equation (4) by an amount Δt_{A} in time. That is, if C^n is an approximation at time t^n, then the approximation at time $t^{n+i/M} = t^n + i\Delta t_{\text{A}}$ $(i = 1, \ldots, M)$ is

$$C^{n+i/M} = \varepsilon_{\text{A}}^{\Delta t_{\text{A}}}(C^{n+(i-1)/M}) \tag{6}$$

The method takes several advection steps per diffusion step. At time $t^{n+1} = t^n + \Delta t_{\text{D}}$, C^{adv} can be expressed in the following recursive form:

$$C^{\text{adv}} = \varepsilon_{\text{A}}^{\Delta t_{\text{A}}}(C^{n+(M-1)/M}) = \varepsilon_{\text{A}}^{\Delta t_{\text{A}}} \circ \varepsilon_{\text{A}}^{\Delta t_{\text{A}}}(C^{n+(M-2)/M}) = \underbrace{\varepsilon_{\text{A}}^{\Delta t_{\text{A}}} \circ \cdots \circ \varepsilon_{\text{A}}^{\Delta t_{\text{A}}}}_{M}(C^n) = (\varepsilon_{\text{A}}^{\Delta t_{\text{A}}})^M(C^n) \tag{7}$$

This result serves as the initial condition for the diffusion operator.

Similarly, let $\varepsilon_{\text{D}}^{\Delta t_{\text{D}}}(C)$ denote the mixed finite element approximation to the pure parabolic equation (5). Then, the operator splitting method may be described as

$$C^{n+1} = \varepsilon_{\text{D}}^{\Delta t_{\text{D}}}((\varepsilon_{\text{A}}^{\Delta t_{\text{A}}})^M(C^n)) \tag{8}$$

This approach, where several advective time steps are computed before taking a single diffusion time step, yields considerable CPU savings, if compared with the case with $M = 1$, where both time steps are equal [3, 19, 20].

2.2. The upwind DG method for the advection equation

The DG method is a high-resolution scheme for advection that achieves high-order accuracy while suppressing spurious oscillations. The method was first introduced in Lesaint and Raviart [31] for solving the neutron transport equation. It was applied to hyperbolic problems in Chavent and Cockburn [32] and was generalized to multidimensional problems while incorporating practical slope limiters in Cockburn and Shu [11].

With the DG finite element method, the advective fluxes are uniquely defined by solving a Riemann problem at the interface of two elements. The DG's solution is shown to be total variation

diminishing (TVD) in Gowda and Jaffré [33]. This property excludes the existence of non-physical oscillations.

In the following, we recall briefly the mathematical developments of the upwind DG method. We adopt an approximation space based on linear polynomials of degree one (P^1-DG method). Additional information about the method can be found in [5].

The physical domain Ω is discretized with triangular elements $\{E\}$. The DG method seeks weak solutions of (4) using the following discontinuous finite element space:

$$V_h = \{v \in L^\infty(\Omega) : v_h|_E \in V(E)\} \tag{9}$$

where $V(E)$ represents the approximation space on the element E.

Basis functions can be discontinuous across inter-element boundaries. The approximate solution $C_h(\mathbf{x}, t)$ is expressed with linear basis functions ϕ_i^E on each element E as follows:

$$C_h(\mathbf{x}, t)|_E = \sum_{i=1}^{3} C_i^E(t)\, \phi_i^E(\mathbf{x}) \tag{10}$$

where $C_i^E(t)$ $(i = 1, \ldots, 3)$ are the three unknown coefficients corresponding to the degrees of freedom. The three unknowns for each element are the average value $\overline{C_h^E}$ of the approximate concentration (10) and its deviations in each space direction $\partial C_h^E/\partial x$ and $\partial C_h^E/\partial y$ with the corresponding interpolation functions [11]:

$$\begin{aligned} C_1^E(t) &= \overline{C_h^E}, \quad \phi_1^E(x, y) = 1 \\ C_2^E(t) &= \frac{\partial C_h^E}{\partial x}, \quad \phi_2^E(x, y) = x - \bar{x}_E \\ C_3^E(t) &= \frac{\partial C_h^E}{\partial y}, \quad \phi_3^E(x, y) = y - \bar{y}_E \end{aligned} \tag{11}$$

Contrarily to the DG finite element method used in Chavent and Jaffré [34] and Siegel *et al.* [3] where unknowns correspond to the concentration at each node of the element, the used approximations do not depend on the geometry of the mesh elements but only on the space dimension.

The variational formulation is obtained by multiplying (4) by the linear test function ϕ_i^E and integrating over the element E:

$$\sum_j \frac{\mathrm{d}C_j^E}{\mathrm{d}t} \int_E \phi_j^E \phi_i^E - \sum_j \int_E C_j^E \phi_j^E \mathbf{V} \cdot \nabla \phi_i^E + \int_{\partial E} C^* \phi_i^E \mathbf{V} \cdot \boldsymbol{\eta}_{\partial E} = 0 \tag{12}$$

The third term corresponds to the boundary integral over the three edges of the element E:

$$\int_{\partial E} C^* \phi_i^E \mathbf{V} \cdot \boldsymbol{\eta}_{\partial E} = \sum_{j=1}^{3} \int_{\Gamma j} C_{\Gamma j}^* \phi_i^E \mathbf{V} \cdot \boldsymbol{\eta}_{\Gamma j} = \sum_{j=1}^{3} \frac{Q_{\Gamma j}^E}{|\Gamma j|} \int_{\Gamma j} C_{\Gamma j}^* \phi_i^E \tag{13}$$

where Γj is the common edge of element E and its adjacent element Ej $(\Gamma j = \partial E \cap \partial Ej)$, $\boldsymbol{\eta}_{\Gamma j}$ is the unit outward normal vector to the edge Γj of length $|\Gamma j|$, and $Q_{\Gamma j}^E$ is the water flux across Γj:

$$Q_{\Gamma j}^E = \int_{\Gamma j} \mathbf{V} \cdot \boldsymbol{\eta}_{\Gamma j} = \mathbf{V} \cdot \boldsymbol{\eta}_{\Gamma j} |\Gamma j| \tag{14}$$

assuming that $\mathbf{V}\cdot\boldsymbol{\eta}_{\Gamma j}$ is constant on Γj [35, 36]. $C^*_{\Gamma j}$ is the concentration over Γj, defined using an appropriate Riemann solver [37], which corresponds to the upstream concentration value:

$$C^*_{\Gamma j} = \lambda^E_{\Gamma j} C_h(\Gamma j, t)|_E + (1-\lambda^E_{\Gamma j}) C_h(\Gamma j, t)|_{Ej} \tag{15}$$

At each edge Γj, we define

$$\lambda^E_{\Gamma j} = \begin{cases} 1 & \text{if } \mathbf{V}\cdot\boldsymbol{\eta}_{\Gamma j} \geqslant 0 \\ 0 & \text{if } \mathbf{V}\cdot\boldsymbol{\eta}_{\Gamma j} < 0 \end{cases}$$

Substituting the three test functions ϕ^E_i in (12) leads to a system of three ordinary differential equations over E.

If we consider an element E and its three adjacent elements $E1$, $E2$, $E3$ (Figure 1), the obtained system can be expressed in the following matrix form:

$$[\mathbf{A}] \begin{pmatrix} \dfrac{\mathrm{d}C^E_1}{\mathrm{d}t} \\ \dfrac{\mathrm{d}C^E_2}{\mathrm{d}t} \\ \dfrac{\mathrm{d}C^E_3}{\mathrm{d}t} \end{pmatrix} = [\mathbf{B}] \begin{bmatrix} C^E_1 \\ C^E_2 \\ C^E_3 \end{bmatrix} - [\mathbf{M}^0] \begin{bmatrix} C^E_1 \\ C^E_2 \\ C^E_3 \end{bmatrix} - [\mathbf{M}^1] \begin{bmatrix} C^{E1}_1 \\ C^{E1}_2 \\ C^{E1}_3 \end{bmatrix} - [\mathbf{M}^2] \begin{bmatrix} C^{E2}_1 \\ C^{E2}_2 \\ C^{E2}_3 \end{bmatrix} - [\mathbf{M}^3] \begin{bmatrix} C^{E3}_1 \\ C^{E3}_2 \\ C^{E3}_3 \end{bmatrix} \tag{16}$$

with

$$A_{i,j} = \int_E \phi^E_j \phi^E_i, \quad B_{i,j} = \int_E \phi^E_j \, \mathbf{V}\cdot\nabla\phi^E_i$$

$$M^0_{i,j} = \lambda^E_{\Gamma 1} \frac{Q^E_{\Gamma 1}}{|\Gamma 1|} \int_{\Gamma 1} \phi^E_i \, \phi^E_j + \lambda^E_{\Gamma 2} \frac{Q^E_{\Gamma 2}}{|\Gamma 2|} \int_{\Gamma 2} \phi^E_i \, \phi^E_j + \lambda^E_{\Gamma 3} \frac{Q^E_{\Gamma 3}}{|\Gamma 3|} \int_{\Gamma 3} \phi^E_i \, \phi^E_j$$

$$M^1_{i,j} = (1-\lambda^E_{\Gamma 1}) \frac{Q^E_{\Gamma 1}}{|\Gamma 1|} \int_{\Gamma 1} \phi^E_i \, \phi^{E1}_j, \quad M^2_{i,j} = (1-\lambda^E_{\Gamma 2}) \frac{Q^E_{\Gamma 2}}{|\Gamma 2|} \int_{\Gamma 2} \phi^E_i \, \phi^{E2}_j$$

$$M^3_{i,j} = (1-\lambda^E_{\Gamma 3}) \frac{Q^E_{\Gamma 3}}{|\Gamma 3|} \int_{\Gamma 3} \phi^E_i \, \phi^{E3}_j$$

All integrals are calculated analytically using (11). For example the mass matrix reduces to

$$[\mathbf{A}] = \begin{pmatrix} |E| & 0 & 0 \\ 0 & I_{xx} & I_{xy} \\ 0 & I_{xy} & I_{yy} \end{pmatrix} \tag{17}$$

with $I_{xx} = \int_E (x-\bar{x}_E)^2$, $I_{yy} = \int_E (y-\bar{y}_E)^2$, and $I_{xy} = \int_E (x-\bar{x}_E)(y-\bar{y}_E)$.

Note that the implicit schemes are usually not used for transient hyperbolic problems due to numerical diffusion.

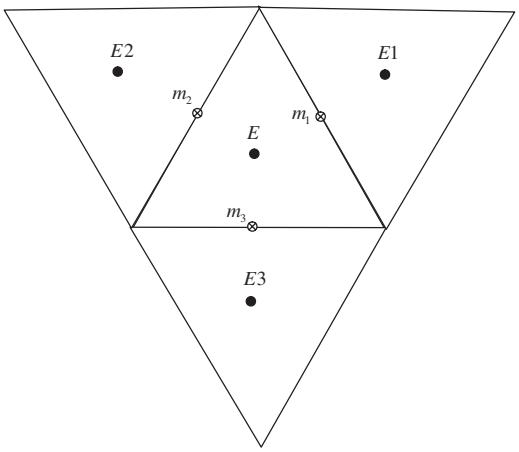

Figure 1. The element E and its three adjacent elements.

The discretization of (16) with an explicit scheme leads to

$$\tilde{C}_E^{n+1} = (\mathbf{I} + \Delta t[\mathbf{A}]^{-1}[\mathbf{B}])C_E^n - \Delta t[\mathbf{A}]^{-1}[\mathbf{M}^0]C_E^n - \Delta t \sum_{j=1}^{3} [\mathbf{A}]^{-1}[\mathbf{M}^j]C_{Ej}^n \tag{18}$$

where $\tilde{C}_E^{n+1} = [(\tilde{C}_1^E, \tilde{C}_2^E, \tilde{C}_3^E)^{n+1}]^{\mathrm{T}}$ contains the unknowns of the element E at the new time level $n+1$ and $C_{Ej}^n = [(C_1^{Ej}, C_2^{Ej}, C_3^{Ej})^n]^T$ the unknowns of the adjacent element Ej at the old time level n.

In (18), the tilde is placed over C to indicate concentrations obtained by the explicit advection before the slope limiting procedure and the plain C indicates limited concentrations.

When the explicit advection scheme is used, the *CFL* criterion has to be fulfilled for all elements in the domain and limiters are necessary to remove unphysical oscillations from the numerical solution.

2.3. The slope limiting

It is known that when using cellwise constant approximations, the numerical diffusion due to upwinding is high enough to keep the scheme stable. However, by using higher-order approximation, the scheme produces non-physical oscillations near shocks. Therefore, the use of an appropriate slope limiter is crucial to ensure the stability of the method.

Many slope limiter techniques for unstructured triangular meshes are proposed in the literature. Chavent and Jaffré [34] introduced a limiter based on Van Leer's MUSCL limiter [38]. The degrees of freedom adopted are the concentrations at the vertices of each element. This technique may fail to smear completely the spurious oscillations and new extrema may be created at the midpoints of the grid edges [39]. To avoid this problem, a slope limiting operator that aims to eliminate oscillations at midpoint edges was proposed in Hoteit *et al.* [39]. Concentrations at vertices are then directly computed by using the reconstructed midpoint edge values. Other slope limiter techniques using the midpoints of edges as degrees of freedom have been developed for unstructured triangular elements [11, 40]. However, oscillations may still appear, depending on the shape of the elements.

In the following, we extend the slope limiter technique developed by Hoteit *et al.* [39] to the family of linear basis and test functions adopted (11). In order to satisfy the local maximum principle, the method ensures that no new extrema are created at the midpoints of the grid edges.

The concentration $\tilde{C}_{m_i}$ at (x_{m_i}, y_{m_i}), the midpoint of the edge Γi (Figure 1), is obtained from (10) and (11):

$$\tilde{C}_{m_i} = \overline{C_h^E} + \frac{\partial \tilde{C}_h^E}{\partial x}(x_{m_i} - \bar{x}_E) + \frac{\partial \tilde{C}_h^E}{\partial y}(y_{m_i} - \bar{y}_E) \tag{19}$$

The limiting is performed only on $\partial \tilde{C}_h^E/\partial x$ and $\partial \tilde{C}_h^E/\partial y$ in order to obtain reconstructed values $(\partial C_h^E/\partial x, \partial C_h^E/\partial y)$. The value $\overline{C_h^E}$ is kept unchanged to preserve the local mass balance.

The reconstructed midpoint values C_{m_i} must have the following two properties:

1. if $\tilde{C}_{m_i}$ is the concentration at the edge Γi, the common edge of elements E and Ei, then C_{m_i} is between $\overline{C_h^E}$ and $\overline{C_h^{Ei}}$, respectively, the mean concentrations in E and Ei,
2. the reconstructed value C_{m_i} is as close as possible to the initial value $\tilde{C}_{m_i}$.

The above optimization problem is equivalent to the following one: For a given $\widetilde{C_E} = (\tilde{C}_{m_1}, \tilde{C}_{m_2}, \tilde{C}_{m_3})$, find $\widehat{C_E} = (C_{m_1}, C_{m_2}, C_{m_3})$ solution of the problem:

$$\begin{aligned} &\min \|\widehat{C_E} - \widetilde{C_E}\|_2 \quad \text{subject to linear constraints} \\ &\min(\overline{C_h^E}, \overline{C_h^{Ei}}) \leqslant C_{m_i} \leqslant \max(\overline{C_h^E}, \overline{C_h^{Ei}}) \quad \text{for } i = 1, \ldots, 3 \end{aligned} \tag{20}$$

This minimization problem is solved using an efficient iterative procedure based on the so-called active set algorithm [41].

Finally, from one reconstructed couple $(C_{m_i}, C_{m_j})_{i \leqslant 3, j \leqslant 3, i \neq j}$, we calculate the new couple $(\partial C_h^E/\partial x, \partial C_h^E/\partial y)$ by solving the following system:

$$\begin{aligned} (x_{m_i} - \bar{x}_E)\frac{\partial C_h^E}{\partial x} + (y_{m_i} - \bar{y}_E)\frac{\partial C_h^E}{\partial y} &= C_{m_i} - \overline{C_h^E} \\ (x_{m_j} - \bar{x}_E)\frac{\partial C_h^E}{\partial x} + (y_{m_j} - \bar{y}_E)\frac{\partial C_h^E}{\partial y} &= C_{m_j} - \overline{C_h^E} \end{aligned} \tag{21}$$

2.4. The mixed finite element for the diffusion equation

The advective part of the transport equation is solved (resolution of (16) for all elements followed by a slope limiting step) M times with a time step Δt_{A}. Then, the obtained results are used as initial concentrations for the diffusion equation. The implicit mixed finite element method [35, 36, 42–45] is used with a single time step $\Delta t_{\mathrm{D}} = M \Delta t_{\mathrm{A}}$. This method is well suited for heterogeneous domains with anisotropic diffusion coefficients. It is locally conservative and can handle general irregular grids.

The diffusion equation (5) is expressed in the following mixed form:

$$\begin{aligned} \frac{C^{n+1} - C^{\mathrm{adv}}}{\Delta t} + \nabla \cdot (\mathbf{q}) &= 0 \\ \mathbf{q} &= -\mathbf{D} \nabla C \end{aligned} \tag{22}$$

The mixed finite element method approximates simultaneously the concentration and the dispersive flux. The discretization of Equation (22) leads to an indefinite system matrix, which is circumvented by hybridization [36, 42]. The system is solved in this case for the concentration on the edges, viewed as Lagrange multipliers. This form is called the mixed hybrid finite element method.

In the following, we recall the assumptions and the main steps for the resolution of the diffusion equation.

The solution is approximated over E by the following quantities:

$$\begin{aligned} C^E &\in \mathbb{R}\text{: the mean value of } C \text{ over the element } E \\ TC_i^E &\in \mathbb{R}\text{: the mean value of } C \text{ over the edge } \Gamma i, \quad i=1,\ldots,3 \\ \mathbf{q}_E &\in \mathbf{X}_E\text{: the approximation of } \mathbf{q}=-\mathbf{D}\nabla C \text{ over } E \end{aligned} \tag{23}$$

where $\mathbf{X}_E$ is the lowest-order Raviart–Thomas space [35, 36, 45] and $\mathbf{q}_E$ may be expressed as

$$\mathbf{q}_E = \sum_{i=1}^{3} Q_{d,i}^E \boldsymbol{\omega}_i^E \tag{24}$$

$Q_{d,i}^E$ denotes the flux leaving E through the ith edge, taken positive outward.

A basis of $\mathbf{X}_E$ on triangles is given by

$$\boldsymbol{\omega}_i^E = \frac{1}{2|E|}\begin{pmatrix} x-x_i^E \\ y-y_i^E \end{pmatrix}, \quad i=1,\ldots,3 \tag{25}$$

where (x_i^E, y_i^E) are the coordinates of the vertices of E and $|E|$ its area.

The variational formulation of the flux law leads to

$$\int_E \boldsymbol{\omega}_i^E \mathbf{D}_E^{-1}\mathbf{q}_E = \sum_{j=1}^{3} Q_{d,j}^E \int_E \boldsymbol{\omega}_i^E \mathbf{D}_E^{-1}\boldsymbol{\omega}_j^E = \int_E \nabla C \boldsymbol{\omega}_i^E = (C^E - TC_i^E) \tag{26}$$

which gives

$$Q_{d,i}^E = \sum_{j=1}^{3} B_{ij}^{-1}(C^E - TC_j^E) \tag{27}$$

with the local matrix $B_{ij} = \int_E \boldsymbol{\omega}_i^E \mathbf{D}_E^{-1}\boldsymbol{\omega}_j^E$.

On the other hand, a finite volume formulation of the first equation in (22) gives

$$\frac{C^{E,n+1} - C^{E,\mathrm{adv}}}{\Delta t}|E| + \sum_{i=1}^{3} Q_{d,i}^E = 0 \tag{28}$$

Then, the final system to solve is obtained by substituting (27) in (28) and writing the continuity of fluxes between two adjacent elements E and Ei:

$$Q_{d,i}^E + Q_{d,i}^{Ei} = 0 \tag{29}$$

This leads to a symmetric positive-definite matrix system, which can be easily solved with standard iterative solvers.

3. THE LOCAL TIME STEPPING SCHEME WITH DG

Stability of the advection discretization is determined by the *CFL* constraint, while the dispersive step, being implicit, is not subject to stability restrictions. The *CFL* constraint on the time step is determined by the ratio of the mesh spacing and the magnitude of the velocity. In oil production applications where injection or production wells are present, for example, fine space discretization is often used around the wells to compute the flow field accurately. Moreover, the magnitude of the velocity is large near the wells and drops sharply as the distance to the well increases. In these cases, the global *CFL* condition turns out to be severe and the standard explicit schemes computationally inefficient [23].

Local time stepping was combined with the finite volume method in Osher and Sanders [21] for one-dimensional conservation laws. A two-dimensional high-resolution version of this method through slope limiters was formulated by Dawson [22] and a second order in time method was introduced by Dawson and Kirby [23]. A similar time integration scheme was used to simulate density-driven flow in porous media by Mazzia and Putti [25]. The local time stepping scheme was successfully used with finite volumes for simulation of microwave antennas in Fumeaux *et al.* [24].

Maximum principles for local time stepping schemes based on first- and second-order time discretizations were proved in a single space dimension in [23]. Moreover, the entropy condition and the TVD property were verified for finite volume methods, which allow spatially varying time steps for general advective flux in [46].

In Flaherty *et al.* [27] and Remacle *et al.* [28], the DG method was used with a recursive multilevel implementation of the local time integration scheme to solve the Euler equations. Based on a local *CFL* condition, mesh elements are clustered into categories and processed sequentially. However, these schemes do not yield a conservative method when applied to the linear advection equation [46].

Numerical results from the literature indicate that local time stepping schemes combined with high-resolution finite volume methods exhibit similar accuracy and stability compared with the global time stepping schemes, with an important reduction of the computational cost [23].

The *CFL* number is defined for each triangular element E as follows [47]:

$$(CFL)_E = \frac{\sum_{j=1}^{3} |Q_{\Gamma j}^E|}{2|E|} \Delta t \tag{30}$$

where $Q_{\Gamma j}^E$ are water fluxes across each edge Γj.

For the first-order DG scheme developed previously, the solution is stable only for $CFL \leqslant 0.5$.

When a single advective time step is taken in the entire computational domain, the global time step is limited by a critical value Δt_c:

$$\Delta t \leqslant \Delta t_c = \min_E \left(\frac{|E|}{\sum_{j=1}^{3} |Q_{\Gamma j}^E|} \right) \tag{31}$$

Small Δt_c values may be necessary for practical problems with unstructured meshes and/or varying velocities.

The basic idea of the local time stepping scheme is to redistribute mesh elements into subdomains where local time steps are used without violating a local stability criterion. Concentration values

in different mesh elements E are updated with different time increments and the stability condition (31) is satisfied locally.

The local time stepping scheme proposed here is an extension of the work of Osher and Sanders [21] and is first illustrated for two local time step subdomains. The physical domain Ω is first divided into two distinct zones Z_1 and Z_2. Let Δt_k denote the local time step satisfying the local *CFL* constraint in zone Z_k, $k=1$ or 2. We assume further that there exists a positive integer L such that $\Delta t_1 = L\Delta t_2$, and consider the following sequence $\{\eta_k\}_{k=0}^{L-1}$:

$$\begin{aligned} \eta_0 &= 0 \\ \eta_k &= \frac{k}{L}, \quad k \in \{1, \ldots, L-1\} \end{aligned} \tag{32}$$

Let p denote the number of adjacent elements of E belonging to the same zone than E.

Elements of the zone Z_2 (zone with the smallest time step) are first updated L times with their local time step Δt_2 as follows:

- solve the upwind DG system:

$$\begin{aligned} \tilde{C}^{n+\eta_k}_{E\in Z_2} = (I + \Delta t[\mathbf{A}]^{-1}[\mathbf{B}])C^{n+\eta_k-1}_{E\in Z_2} - \Delta t[\mathbf{A}]^{-1}[\mathbf{M}^0]C^{n+\eta_k-1}_{E\in Z_2} \\ -\Delta t_2 \sum_{j=1}^{p} [\mathbf{A}]^{-1}[\mathbf{M}^j]C^{n+\eta_k-1}_{Ej\in Z_2} - \Delta t_2 \sum_{j=p+1}^{3} [\mathbf{A}]^{-1}[\mathbf{M}^j]C^{n}_{Ej\in Z_1} \end{aligned} \tag{33}$$

- calculate the new values $C^{n+\eta_k}_{E\in Z_2}$ by limiting the slope of $\tilde{C}^{n+\eta_k}_{E\in Z_2}$ using the mean values $\overline{C}^{n+\eta_k}_{E\in Z_2}$ and $\overline{C}^{n}_{E\in Z_1}$:

$$C^{n+\eta_k}_{E\in Z_2} = \Im(\tilde{C}^{n+\eta_k}_{E\in Z_2}, \overline{C}^{n+\eta_k}_{E\in Z_2}, \overline{C}^{n}_{E\in Z_1}) \tag{34}$$

  where $\Im$ is the slope limiting operator.

Elements of the zone Z_1 are then updated with a single time step Δt_1 as follows:

- solve the upwind DG system:

$$\begin{aligned} \tilde{C}^{n+1}_{E\in Z_1} = (I + \Delta t[\mathbf{A}]^{-1}[\mathbf{B}])C^{n}_{E\in Z_1} - \Delta t[\mathbf{A}]^{-1}[\mathbf{M}^0]C^{n}_{E\in Z_1} - \Delta t_1 \sum_{j=1}^{p} [\mathbf{A}]^{-1}[\mathbf{M}^j]C^{n}_{Ej\in Z_1} \\ -\Delta t_1 \sum_{j=p+1}^{3} [\mathbf{A}]^{-1}[\mathbf{M}^j] \left(\frac{1}{L} \sum_{k=0}^{L-1} C^{n+\eta_k}_{Ej\in Z_2} \right) \end{aligned} \tag{35}$$

- calculate the new values $C^{n+1}_{E\in Z_1}$ by limiting the slope of $\tilde{C}^{n+1}_{E\in Z_1}$ using the mean values $\overline{C}^{n+\eta_L}_{E\in Z_2}$ and $\overline{C}^{n+1}_{E\in Z_1}$:

$$C^{n+1}_{E\in Z_1} = \Im(\tilde{C}^{n+1}_{E\in Z_1}, \overline{C}^{n+1}_{E\in Z_1}, \overline{C}^{n+\eta_L}_{E\in Z_2}) \tag{36}$$

This technique advances first the solution in the small time step region (for $E \in Z_2$) L times, using the solution at time t^n in the neighbor elements Ej of large time steps ($Ej \in Z_1$). The concentration computed at the interface is accumulated and averaged. This average concentration is used as the

edge concentration on the element with the large time step (for $E \in Z_1$). Two main differences appear with the DG method compared with the standard finite volume method used in [48, 49]:

(i) an extra term (the second term) appears in the variational formulation (12);
(ii) the boundary integral (13) on Γj (the common edge of elements E and Ej) is different when working on E or Ej.

The procedure described above for two zones can be generalized to more zones.

We define the total time step, Δt_{D}, which corresponds to the time step used for the implicit diffusive part of the equation. The integer K is the time step multiplier for each element. To avoid a too high contrast in time steps between adjacent elements, we choose $K=2$.

The smaller time step Δt_{s} is defined by: (i) Δt_{s} is smaller than the critical value Δt_{c} defined by (31) and (ii) Δt_{s} is the largest time step such that Δt_{D} is a power of K multiples of Δt_{s}:

$$\begin{aligned} &\Delta t_{\mathrm{s}} \leqslant \Delta t_{\mathrm{c}} \\ &\Delta t_{\mathrm{s}} = \max_{m>0} \left(\frac{\Delta t_{\mathrm{D}}}{K^{m-1}} \right) \end{aligned} \tag{37}$$

Each element E will take a power of K multiples of Δt_{s}:

$$\Delta t_E = K^{\ell-1} \Delta t_{\mathrm{s}} \tag{38}$$

where $\ell > 0$ is the largest integer that satisfies for each element the local *CFL* condition:

$$K^{\ell-1} \Delta t_{\mathrm{s}} \leqslant \left(\frac{|E|}{\sum_{j=1}^{3} |Q_{\Gamma j}^{E}|} \right) \tag{39}$$

Elements can then be clustered into zones Z_ℓ having the same local time step $K^{\ell-1}\Delta t_{\mathrm{s}}$.

Once elements are grouped into zones according to their local time steps, a scheduling is needed in order to define the sequence of computations carried out on the elements of each zone. A scheduling for transient inviscid flows was proposed in [28], which needs interpolation and is therefore non-conservative. The one we use includes appropriate step coordination to avoid interpolation and, therefore, remains mass conservative.

As an example, we consider the case with three different zones; therefore, the largest time step that equals $4\Delta t_{\mathrm{s}}$ is obtained for Z_3. Elements of Z_1 are first updated twice according to their local time steps. Elements of Z_2 are then advanced once using the required available values of elements Z_1 (Figure 2(a)). The same procedure is repeated once (Figure 2(b)) and finally the elements of Z_3 are computed with a single operation (Figure 2(c)). The final sequence order for processing the sets from t to $t+4\Delta t_{\mathrm{s}}$ is

$$S_3 = \{Z_1, Z_1, Z_2, Z_1, Z_1, Z_2, Z_3\} \tag{40}$$

Notice that $S_2 = \{Z_1, Z_1, Z_2\}$.

The sequence can be obtained recursively for n zones as follows:

$$S_n = \{S_{n-1}, S_{n-1}, Z_n\} \quad \text{with} \begin{cases} S_1 = Z_1 \\ \mathrm{n} \geqslant 2 \end{cases} \tag{41}$$

Note that a similar construction is proposed in [29] for wave propagation problems using an explicit leap-frog time discretization.

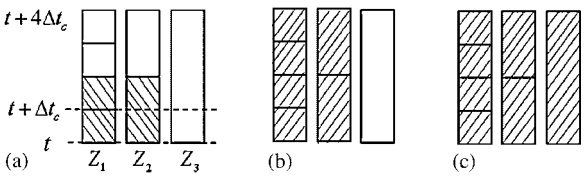

Figure 2. Local time stepping sequence for $\ell_{\max}=3$. Elements of each zone are advanced sequentially in time with their own time step.

4. EFFICIENCY OF DG/MIXED METHODS WITH LOCAL TIME STEPS

In this part, we study the efficiency of the model based on DG/mixed finite elements and local time stepping procedure. Three test cases with unstructured meshes are used to evaluate the benefit in terms of accuracy and efficiency of the developed model.

Test cases represent transport of a tracer in uniform and non-uniform flow fields and a simplified case of saltwater intrusion for coastal aquifers.

Before simulating the transport equation, the flow equation is first solved with the mixed hybrid finite element method on triangles [44, 45], which gives accurate velocities with continuous normal component across the inter-element boundary.

4.1. Test case 1: transport in a uniform flow field with local mesh refinement

In this section, the local time stepping scheme is used for the resolution of the transport problem in a rectangular spatial domain Ω. The domain is portioned into unstructured triangular elements with 2070 nodes and 4004 elements as shown in Figure 3. The mesh refinement is located close to transverse concentration fronts in order to increase the sensitivity of the spatial resolution. The flow is one-dimensional, horizontal, and uniform ($v_x=1.0\,\mathrm{m/s}$, $v_y=0\,\mathrm{m/s}$). The diffusion tensor is anisotropic and diagonal, with D_l being its component in the fluid flow direction and D_t in the transverse direction. The boundary conditions are of Dirichlet type at the inflow with

$$C(0,y)=0 \quad \forall y\in[0,12[$$

$$C(0,y)=1 \quad \forall y\in[12,28]$$

$$C(0,y)=0 \quad \forall y\in]28,40]$$

A zero diffusive flux is prescribed at the outflow boundary. The results are given for different ranges of grid Peclet number using the following diffusion parameters:

- Sim1: $D_\mathrm{l}=0.002\,\mathrm{m^2/s}$, $D_\mathrm{t}=0.0005\,\mathrm{m^2/s}$, i.e. a grid Peclet number varying from 101 to 1467.
- Sim2: $D_\mathrm{l}=0.2\,\mathrm{m^2/s}$, $D_\mathrm{t}=0.05\,\mathrm{m^2/s}$, i.e. a grid Peclet number varying from 1.01 to 14.67.
- Sim3: $D_\mathrm{l}=2.0\,\mathrm{m^2/s}$, $D_\mathrm{t}=0.5\,\mathrm{m^2/s}$, i.e. a grid Peclet number varying from 0.101 to 1.467.

For all simulations, we have $\Delta t_\mathrm{s}=0.0375\,\mathrm{s}$ and $\Delta t_\mathrm{D}=0.6\,\mathrm{s}$. With the global time stepping implementation, all elements take the same time step Δt_s for advection. With the local time stepping procedure, the elements are portioned into zones (Figure 4). Each element takes either Δt_s or a local time step that is $2^0, 2^1, \ldots, 2^4$ times greater and which verifies the local *CFL* constraint.

For all the subsequent simulations, we consider the solution at simulation time $T=60\,\mathrm{s}$. Simulations performed with both global and local time stepping schemes are compared with the analytical

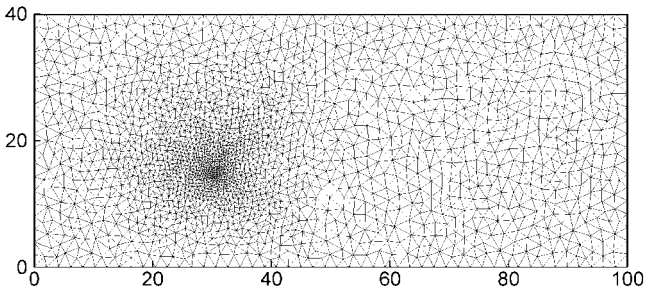

Figure 3. The physical domain Ω discretized with unstructured triangular elements for the transport problem in a uniform flow.

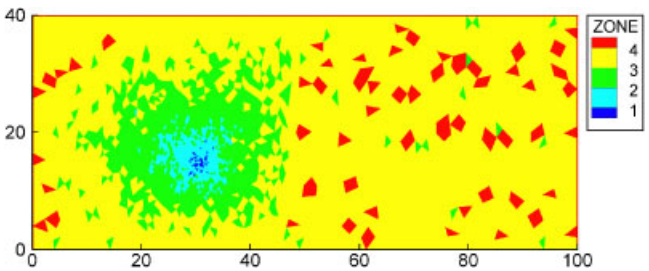

Figure 4. Distribution of zones of constant time step with five levels of time refinement for the transport problem in a uniform flow field.

solution given in Leij Feike and Dane [50]. In Sim1, the transport is advection-dominated. The sharp front is well calculated at different simulation times and numerical stability is observed with both the global and the local time stepping schemes (Figure 5). Longitudinal profiles at $y = 15\,\mathrm{m}$ (Figure 6) show that the global time stepping scheme introduces more numerical diffusion than the local time stepping scheme. This point will be studied with more details in the next test case problem. When diffusion becomes significant (Sim2 and Sim3), the longitudinal and transverse profiles of analytic, global, and local time stepping schemes are very close (Figures 7–10).

Table I gives the root mean square (RMS) error and the Max error defined by

$$\text{RMS error} = \frac{1}{N_e}\sqrt{\sum_{i=1}^{N_e}(\overline{C}_i^{\text{numerical}} - \overline{C}_i^{\text{analytical}})^2} \tag{42}$$

$$\text{Max error} = \max_i |\overline{C}_i^{\text{numerical}} - \overline{C}_i^{\text{analytical}}| \tag{43}$$

where N_e is the total number of elements.

Table I shows that errors obtained with both time integration schemes are of the same order of magnitude. Max errors obtained with the local time integration scheme are slightly inferior to those obtained with the global time integration scheme. Both schemes are also mass conservative since they lead to an exact mass balance.

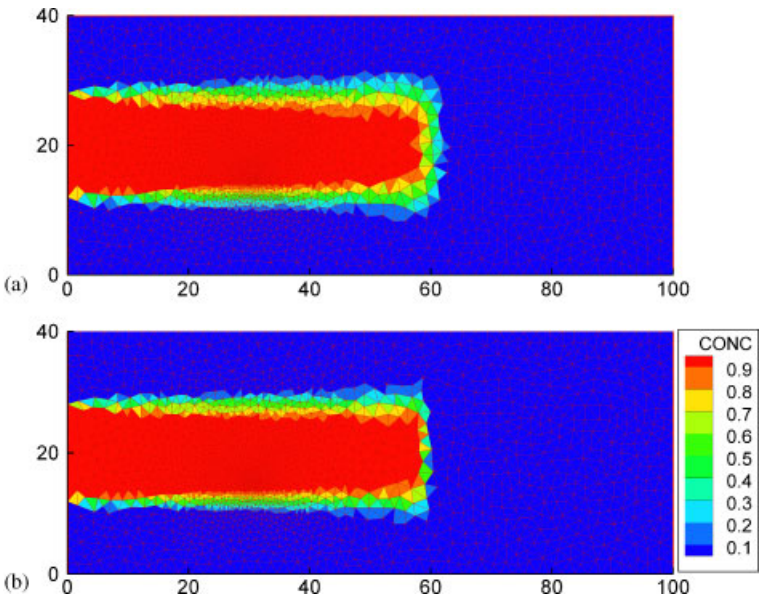

Figure 5. Results for the upwind DG method with (a) the global time stepping scheme and (b) the local time stepping scheme for Sim1.

The computational efficiency, which is the main objective of locally varying time step schemes, is also studied for this test problem. It can be roughly estimated by the number of computations that have to be performed within one diffusion time step Δt_{D}. For the global time stepping scheme, the total number of computations N_{G} is

$$N_{\mathrm{G}} = n \sum_i N_{Ei} \quad \text{with } N_{\mathrm{e}} = \sum_i N_{Ei} \tag{44}$$

where Δt_{s} is the smallest time step defined by (37), N_{Ei} is the number of elements in zone Z_i, and n is an integer that satisfies $\Delta t_{\mathrm{D}} = n \Delta t_{\mathrm{s}}$.

For the local time stepping scheme, the total number of computations N_{L} is

$$N_{\mathrm{L}} = n \sum_i N_{Ei} / K^{i-1} \tag{45}$$

with $K = 2$ in our case (see (37)–(39)).

The theoretical speedup of the method is defined by

$$\frac{N_{\mathrm{G}}}{N_{\mathrm{L}}} = \sum_i N_{Ei} \Big/ \sum_i (N_{Ei} / K^{i-1}) \tag{46}$$

The actual speedup can be lower because of the numerous tests carried out in the code and it depends on the skill of the programmer. Table I gives the actual speedup of the local time stepping scheme: the ratio between the computational times of the global and local time stepping schemes. The local time stepping scheme uses five zones with different time steps (Figure 4), which leads

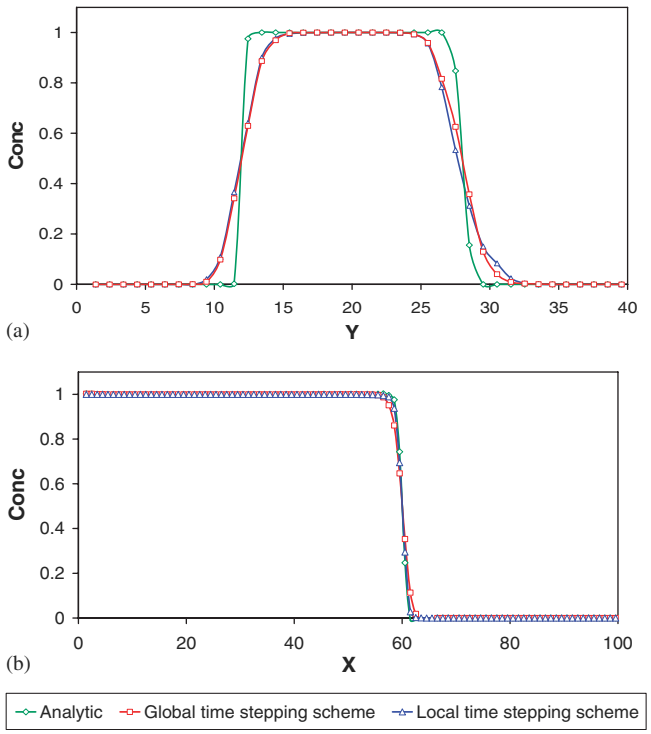

Figure 6. Analytic solution and results for the upwind DG method with the local and global time stepping schemes: (a) transverse profile at $y=15$ and (b) longitudinal profile at $x=30$ for Sim1.

to an average actual speedup for the three cases of about 3.76. The theoretical speedup is 4.1 for this example.

Figure 11 shows continuous improvement of the average actual speedup when the number of zones is increased. The benefit of increasing the number of zones is more significant at the beginning. As shown in Figure 11, the benefit of the local time stepping scheme is more important when we go up from two to three zones than from four to five zones. For this test problem, the maximum average speedup is about 4 and is reached with four zones of different time steps.

Simulations of this first transport problem with local mesh refinement and a uniform flow field show that the upwind DG method with local time stepping procedure is stable, accurate, and mass conservative. It leads to a significant reduction of the computational cost and is shown to be efficient for a large range of grid Peclet numbers.

4.2. Test case 2: transport in a non-uniform flow field with local mesh refinement

We consider now a transport problem for a non-uniform flow field with a local mesh refinement as shown in Figure 12. The problem corresponds to the transport of a two-dimensional rotating Gaussian pulse, which is a very standard test case. The spatial domain is $\Omega=(0,1)\times(0,1)$, the rotation field is $V_1(x,y)=2-4y\,\mathrm{m/s}$, $V_2(x,y)=2-4x\,\mathrm{m/s}$, and the final time for the simulation is $T=(\pi/2)\,\mathrm{s}$, which corresponds to the time period required for one complete rotation. The initial

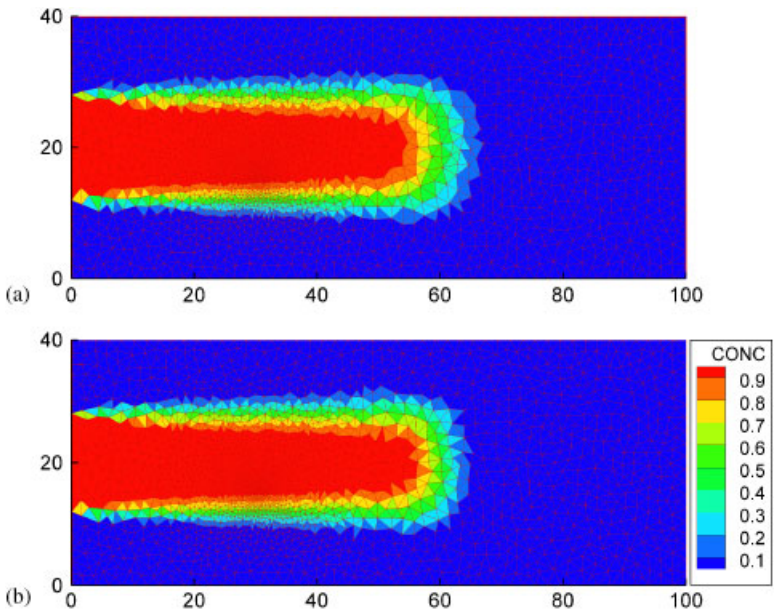

Figure 7. Results for the upwind DG method with (a) the global time stepping scheme and (b) the local time stepping scheme for Sim2.

concentration is given by

$$C_0(x,y)=\exp\left(-\frac{(x-x_C)^2+(y-y_C)^2}{2\sigma^2}\right) \tag{47}$$

where x_C, y_C, and σ are the center and standard deviations of the Gaussian pulse. The corresponding analytical solution with a constant diffusion coefficient D is given by

$$C(x,y,t)=\frac{2\sigma^2}{2\sigma^2+4Dt}\exp\left(-\frac{(\bar{x}-x_C)^2+(\bar{y}-y_C)^2}{2\sigma^2+4Dt}\right) \tag{48}$$

where $\bar{x}=x\cos(4t)+y\sin(4t)$ and $\bar{y}=-x\sin(4t)+y\cos(4t)$.

This problem provides a transport equation with variable velocity and known analytical solution. In the numerical experiments, we choose $D=10^{-8}\,\mathrm{m}^2/\mathrm{s}$, $x_C=0.25\,\mathrm{m}$ L, $y_C=0.5\,\mathrm{m}$, and $\sigma=0.0447\,\mathrm{m}^2/\mathrm{s}$.

The problem is discretized with seven zones of different time steps as shown in Figure 12. Results of simulations are plotted in Figure 13. Table II gives the maximum value of the concentration, the RMS error, and the maximum error for both the global and local time stepping schemes.

The initial concentration defined by (47) has a minimum value 0 and a maximum value 1. Owing to the very small diffusion coefficient, the maximum value of the analytical solution (48) after one complete rotation is kept almost constant (its value is 0.9998).

With both schemes the maximum value of the simulated concentration after one rotation is less than that of the analytical concentration. This phenomenon is due to the numerical diffusion present in all upwind methods. However, Table II shows that the maximum value of the concentration

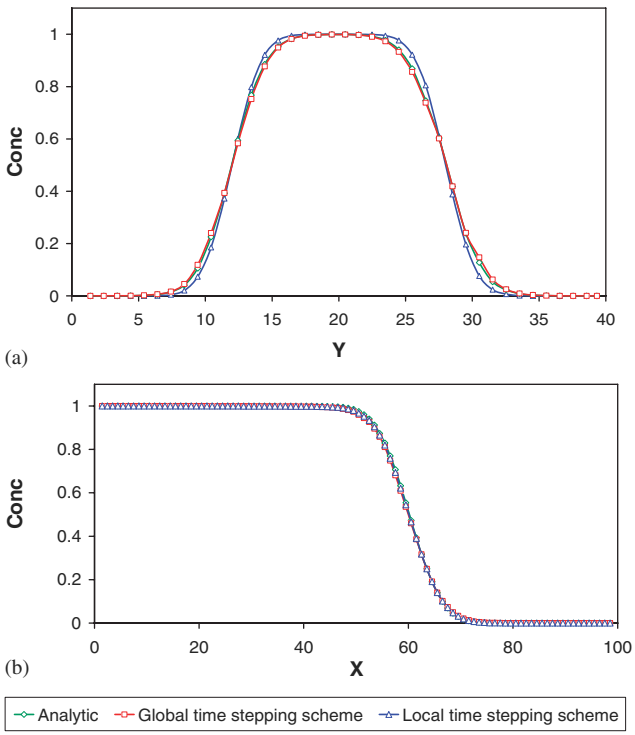

Figure 8. Analytic solution and results for the upwind DG method with the local and global time stepping schemes: (a) transverse profile at $y = 15$ and (b) longitudinal profile at $x = 30$ for Sim2.

with the local time stepping scheme is higher than that with the global time stepping scheme. The numerical diffusion with the local time stepping scheme is therefore less important than that with the global time stepping scheme. This phenomenon is due to the number of computations required to obtain the final solution. Indeed, it is known that the upwind DG method gives stable results if the *CFL* constraint is verified but introduces small numerical diffusion smearing the front. This numerical diffusion is therefore proportional to the total number of performed computations. For our test case problem, the upwind DG method with the local time stepping scheme requires fewer computations since each element is updated with its appropriate time step with respect to the local *CFL* condition. Results are therefore more accurate (with less numerical diffusion) than that with the global time stepping scheme.

The actual speedup for this case is about 4 (the theoretical speedup is 4.9), which emphasizes the greater efficiency of the upwind DG method with the local time stepping procedure.

4.3. Test case 3: saltwater intrusion problem with production well

In this test case, we extend the local time stepping procedure to a transient flow field. The clustering of the elements in zones and the number of zones with an identical time step may change for each new flow field. The studied example deals with solute transport in porous media induced by density-driven flow. When density variations are significant, flow and transport are strongly coupled.

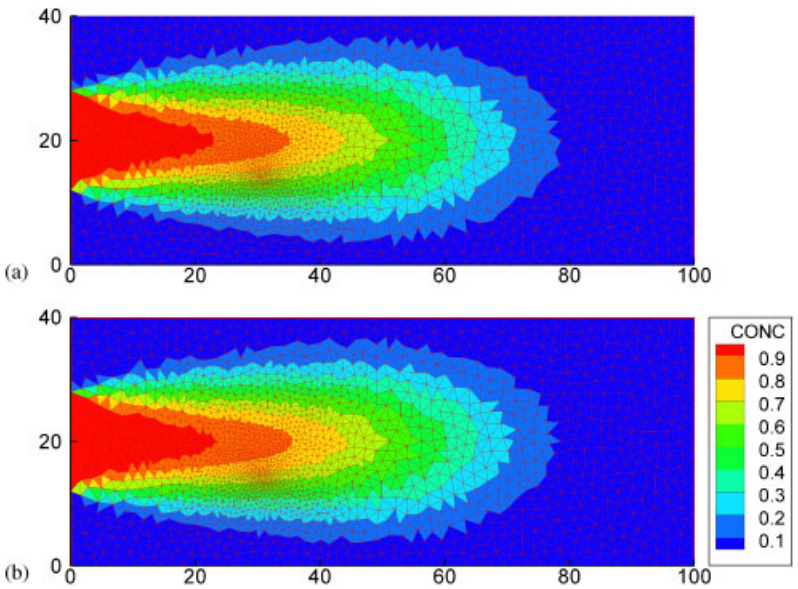

Figure 9. Results for the upwind DG method with (a) the global time stepping scheme and (b) the local time stepping scheme for Sim3.

At each time step, we have to solve the non-linear system of partial differential equations describing the mass conservation of the fluid, the generalized Darcy's law, and the transport equation of solute mass fraction [51]:

$$\begin{aligned} \rho S\frac{\partial h}{\partial t}+\varepsilon\frac{\partial \rho}{\partial C_{\mathrm{m}}}\frac{\partial C_{\mathrm{m}}}{\partial t}+\rho\nabla\cdot\mathbf{q}&=0\\ \mathbf{q}&=-\mathbf{K}\left(\nabla h+\frac{\rho-\rho_0}{\rho_0}\nabla z\right)\\ \rho&=\rho_0+(\rho_1-\rho_0)C_{\mathrm{m}}\\ \varepsilon\frac{\partial C_{\mathrm{m}}}{\partial t}+\mathbf{q}\cdot\nabla C_{\mathrm{m}}-\nabla\cdot\mathbf{D}\nabla C_{\mathrm{m}}&=0 \end{aligned} \tag{49}$$

where P is the fluid pressure [$\mathrm{ML^{-1}T^{-2}}$], $\mathbf{q}$ is Darcy's velocity [$\mathrm{LT^{-1}}$], ε is the porosity [–], $\mathbf{K}=\mathbf{k}\rho_0 g/\mu$ is the hydraulic conductivity tensor [$\mathrm{LT^{-1}}$], $\mathbf{k}$ is the permeability tensor [$\mathrm{L^2}$], g is the gravity acceleration [$\mathrm{LT^{-2}}$], ρ is the fluid density [$\mathrm{ML^{-3}}$], μ is the fluid dynamic viscosity [$\mathrm{ML^{-1}T^{-1}}$], C_{m} is the solute mass fraction [M. salt/M. fluid], $h=P/\rho_0 g+z$ is the equivalent freshwater head, S is the specific mass storativity related to head changes [$\mathrm{L^{-1}}$], ρ_1 is the seawater fluid density, and ρ_0 and μ_0 are the density and viscosity of freshwater.

A simplified problem of saltwater intrusion in a coastal aquifer with a pumping well is studied here. The problem describes the advance of a saltwater front in a rectangular $2\,\mathrm{m}\times 1\,\mathrm{m}$ confined aquifer initially charged with freshwater. Boundary conditions are those of the standard Henry problem and correspond to a hydrostatic head at the right-hand side with a density of $\rho_1=1025\,\mathrm{kg/m^3}$ for seawater. At the left boundary, a constant freshwater ($\rho_0=1000\,\mathrm{kg/m^3}$) flux is

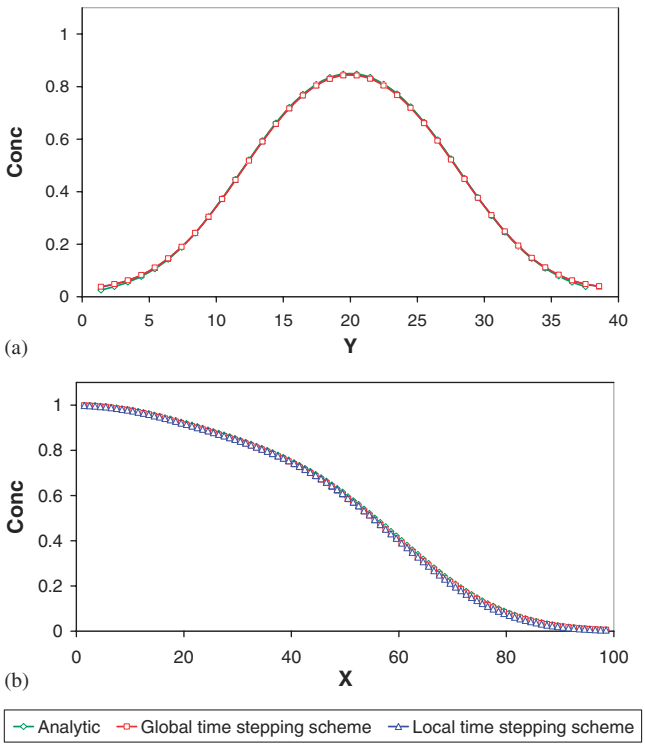

Figure 10. Analytic solution and results for the upwind DG method with the local and global time stepping schemes: (a) transverse profile at $y=15$ and (b) longitudinal profile at $x=30$ for Sim3.

Table I. Results for the transport problem in a uniform flow field with local mesh refinement.

	RMS error	Max error	Actual speedup
Case 1			
GT	1.60×10^{-3}	0.55	
LT	1.66×10^{-3}	0.53	3.8
Case 2			
GT	3.01×10^{-4}	0.18	
LT	3.8×10^{-4}	0.18	3.8
Case 3			
GT	6.81×10^{-5}	9.45×10^{-2}	
LT	7.83×10^{-5}	9.0×10^{-2}	3.7

GT, global time stepping scheme; LT, local time stepping scheme.

applied with a rate of $Q=6.6\times10^{-5}\mathrm{m}^3/\mathrm{s}$. A production well (point sink) is located at $(1, 0.3\,\mathrm{m})$ and water is extracted with a constant rate $Q_s=10^{-4}\,\mathrm{m}^3/\mathrm{s}$. The parameter values are listed in Table III. The rectangular domain is discretized with an unstructured triangular mesh of 1631 nodes

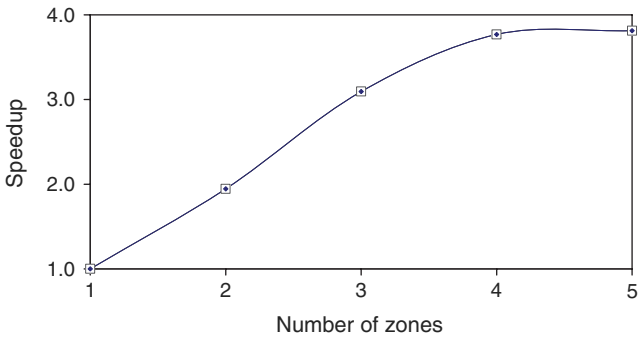

Figure 11. Actual speedup obtained for the transport problem in a uniform flow field with local mesh refinement.

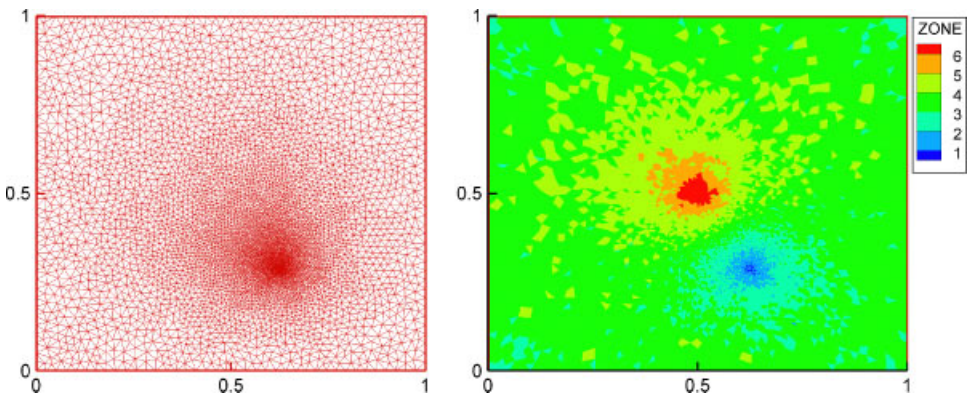

Figure 12. Mesh refinement and distribution of zones of constant time steps with seven levels of time refinement for the transport problem in a non-uniform flow field.

and 3142 elements. Fine spatial discretization is adopted in the vicinity of the production well to obtain accurate velocities (Figure 14). Simulations are performed with final time $T = 4000\,\mathrm{s}$.

Since the velocity field is influenced by density variation, the local *CFL* (for each element of the mesh) is no longer constant in time. This implies that the spatial distribution of the different time steps varies in time (Figure 15). Therefore, we have a dynamic partition of the zones. The total number of zones varies between 5 and 11 during the simulation. Because of mesh refinement and large velocities near the well, very small local time steps are required in the vicinity of the well. The smallest time step Δt_s is used only for the element containing the production well. Time steps that are at least two times greater (Figure 15) are used for the other elements.

The results with the local time stepping are very close to the global time step results (Figure 16). During the simulations, no stability problem was encountered and the mass is exactly conserved. The local time stepping scheme is much more efficient than the global time stepping scheme, and the average actual speedup is greater than 20 for this test case. This gain could be much more

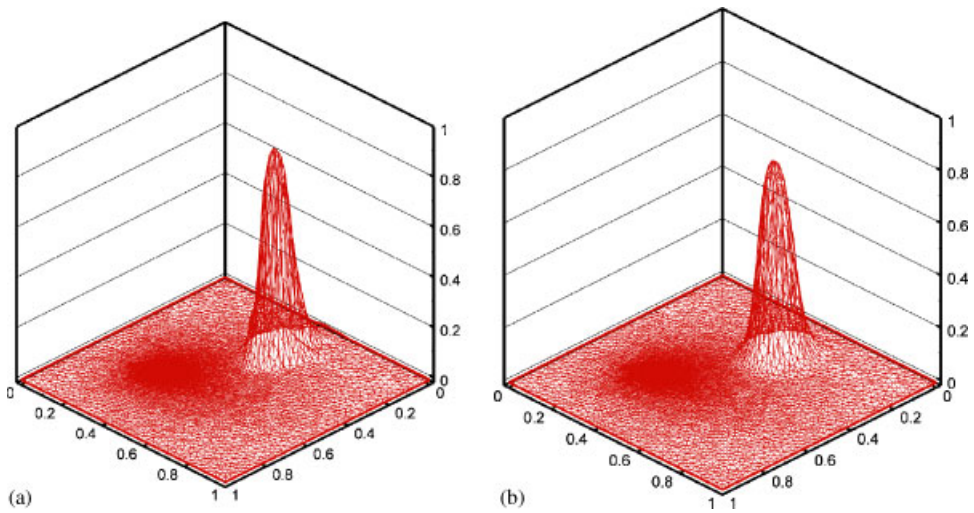

Figure 13. The rotating pulse after one complete revolution obtained with (a) the local time stepping scheme and (b) the global time stepping scheme for the transport problem in a non-uniform flow field.

Table II. Results for the two-dimensional rotating Gaussian pulse with unstructured mesh.

	$C_{\max}$	RMS error	Max error	Actual speedup
Global time stepping scheme	0.74	9.8×10^{-5}	0.25	
Local time stepping scheme	0.83	1.2×10^{-4}	0.32	4.0

Table III. Parameters and boundary conditions for the saltwater intrusion problem with production well.

Permeability	$k_x = k_y = 1.0204\times10^{-9}\,\mathrm{m}^2$
Porosity	$\phi = 0.35$
Dispersivity	$\alpha_L = \alpha_T = 0\,\mathrm{m}$
Molecular diffusion coefficient	$D_{\mathrm{m}} = 3.772\times10^{-6}\,\mathrm{m}^2/\mathrm{s}$
Boundary conditions for flow	Hydrostatic pressure at the right-hand side
	Constant flux at the inflow boundary: $Q = 6.6\times10^{-5}\,\mathrm{kg/m}^3$
	No flow along the top and bottom
Boundary conditions for transport	$\rho_0 = 1000\,\mathrm{kg/m}^3$ on the left boundary
	$\rho_1 = 1025\,\mathrm{kg/m}^3$ on the left boundary
	Zero concentration gradient along the top and the bottom

important in the case of highly unstructured mesh with smaller elements and/or a higher pumping rate Q_{s}.

Results for this non-linear problem show the high efficiency of the developed fully automated local time stepping procedure.

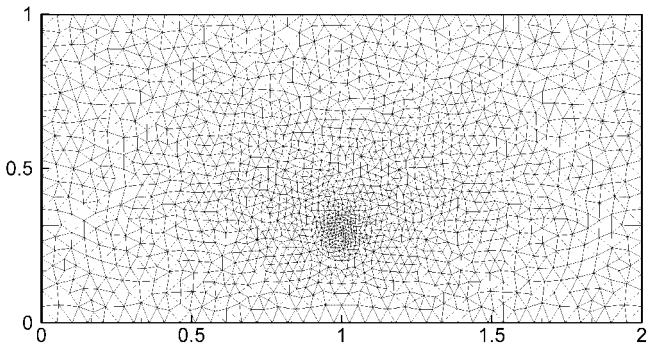

Figure 14. Local mesh refinement in the vicinity of the production well for the saltwater intrusion problem.

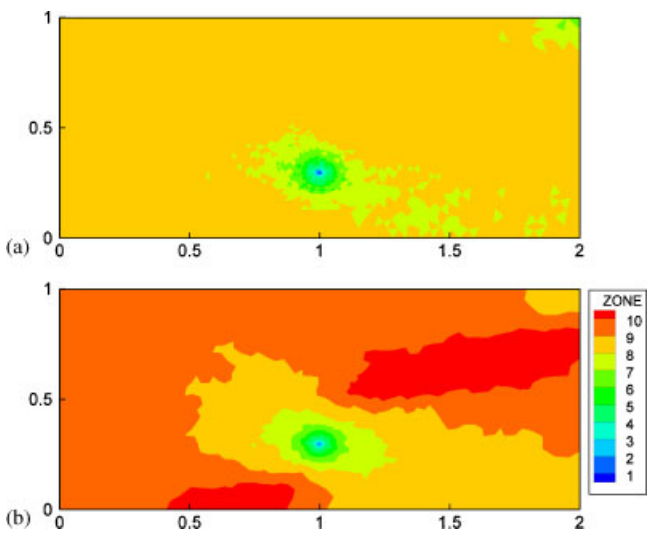

Figure 15. Distribution of zones of constant time steps at (a) $T = 1500\,\mathrm{s}$ and (b) $T = 4000\,\mathrm{s}$ for the saltwater intrusion problem with production well.

5. CONCLUSION

A combination of an explicit upwind DG method with an implicit mixed finite element method is associated with a local time stepping procedure for the resolution of the advection–diffusion equation on unstructured triangular grids. The local time stepping procedure is based on a fully automatic partitioning of the computational domain into subsets where local time steps can be applied without deteriorating stability.

Numerical experiments show that the developed model provides accurate results and is efficient for a large range of grid Peclet numbers: the computational time is significantly reduced, the procedure is mass conservative, and, compared with the usual global time stepping approach, less numerical diffusion has been observed for highly advective problems.

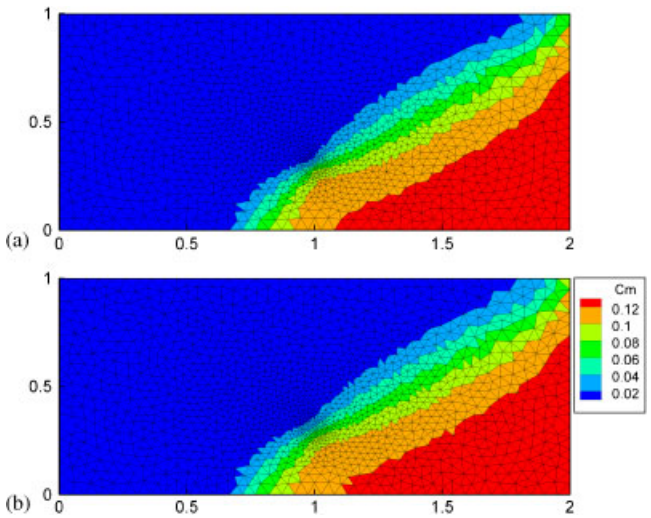

Figure 16. Results for the upwind DG method with (a) the global time stepping scheme and (b) the local time stepping scheme for the saltwater intrusion problem with production well.

The model was also tested on a transient flow field due to density-driven flow. For this non-linear problem, the velocity field changes at each iteration, which requires a dynamic partitioning of the domain (zone locations and number of zones). The results point out the efficiency of the local time stepping procedure for this type of problem for which the usual global time stepping procedure is known to be highly CPU consuming. For this specific test case, the local time stepping procedure is 20 times faster than the global time stepping scheme.

ACKNOWLEDGEMENTS

This work is based upon research supported by ANDRA (French agency for nuclear waste management). The financial support of ANDRA during the thesis of Ch. P. El Soueidy was greatly appreciated. The authors would also like to thank the anonymous reviewers for their helpful comments.

REFERENCES

1. Godlewski E, Raviart P-A. *Numerical Approximation of Hyperbolic Systems of Conservation Laws*. Applied Mathematical Sciences. Springer: New York, Berlin, 1996.
2. Huyakorn PS, Pinder GF. *Computational Methods in Subsurface Flow*. Academic Press: San Diego, CA, 1983.
3. Siegel P, Mosé R, Ackerer P, Jaffre J. Solution of the advection–diffusion equation using a combination of discontinuous and mixed finite elements. *International Journal for Numerical Methods in Fluids* 1997; **24**: 595–613.
4. Aizinger V, Dawson C, Cockburn B, Castillo P. The local discontinuous Galerkin method for contaminant transport. *Advances in Water Resources* 2001; **24**:73–87.
5. Cockburn B. Discontinuous Galerkin methods. *Journal of Applied Mathematics and Mechanics* 2003; **11**:731–754.
6. Reed WH, Hill TR. Triangular mesh methods for the neutron transport equation. *Technical Report LA-UR-73-479*, Los Alamos Scientific Laboratory, 1973.
7. Cockburn B, Shu CW. TVB Runge–Kutta local projection discontinuous Galerkin finite element method for conservation laws II: one dimensional systems. *Journal of Computational Physics* 1989; **84**:90–113.

8. Cockburn B, Shu CW. The Runge–Kutta local projection P1-discontinuous Galerkin finite element method for scalar conservation laws. *Mathematical Modelling and Numerical Analysis* 1991; **25**:337–361.
9. Wheeler MF. An elliptic collocation finite element method with interior penalties. *SIAM Journal on Numerical Analysis* 1978; **15**:152–161.
10. Oden JT, Babuska I, Baumann CE. A discontinuous hp finite element method for diffusion problems. *Journal of Computational Physics* 1998; **146**:491–519.
11. Cockburn B, Shu CW. The Runge–Kutta discontinuous Galerkin method for conservation laws V. *Journal of Computational Physics* 1998; **141**:199–224.
12. Rivière B, Wheeler MF, Girault V. Improved energy estimates for interior penalty, constrained and discontinuous Galerkin methods for elliptic problems. Part I. *Computational Geosciences* 1999; **3**:337–360.
13. Rivière B, Wheeler MF, Girault V. A priori error estimates for finite element methods based on discontinuous approximation spaces for elliptic problem. *SIAM Journal on Numerical Analysis* 2001; **39**:902–931.
14. Arnold DN, Brezzi F, Cockburn B, Marini LD. Unified analysis of discontinuous Galerkin methods for elliptic problems. *SIAM Journal on Numerical Analysis* 2002; **39**:1749–1779.
15. Li F, Shu CW. A local-structure-preserving local discontinuous Galerkin method for the Laplace equation. *Methods and Applications of Analysis* 2006; **13**:215–234.
16. Kirby R. Local time stepping and a posteriori error estimates for flow and transport in Porous Media. *Ph.D. Thesis*, University of Texas at Austin, 2000.
17. Dawson C. Godunov-mixed methods for advection flow problems in one space dimension. *SIAM Journal on Numerical Analysis* 1991; **28**:1282–1309.
18. Dawson C. Godunov-mixed methods for advection–diffusion equations in multidimensions. *SIAM Journal on Numerical Analysis* 1993; **30**:1315–1332.
19. Mazzia A, Bergamaschi L, Putti M. A time-splitting technique for the advection–dispersion equation in groundwater. *Journal of Computational Physics* 2000; **157**:181–198.
20. Ackerer P, Younes A, Mosé R. Modelling variable density flow and solute transport in porous medium: 1. Numerical model and verification. *Transport in Porous Media* 1999; **35**:345–373.
21. Osher S, Sanders R. Numerical approximations to nonlinear conservation laws with locally varying time and space Grids. *Mathematics of Computation* 1983; **41**:321–336.
22. Dawson C. High resolution upwind–mixed finite element methods for advection–diffusion equations with variable time-stepping. *Numerical Methods for Partial Differential Equations* 1995; **11**:525–538.
23. Dawson C, Kirby R. High resolution schemes for conservation laws with locally varying time steps. *SIAM Journal on Scientific Computing* 2001; **22**:2256–2281.
24. Fumeaux C, Baumann D, Leuchtmann P, Vahldieck R. A generalized local time-step scheme for efficient FVTD simulations in strongly inhomogeneous meshes. *IEEE Transactions on Microwave Theory and Techniques* 2004; **52**:1067–1076.
25. Mazzia A, Putti M. High order Godunov mixed methods on tetrahedral meshes for density driven flow simulations in porous media. *Journal of Computational Physics* 2005; **208**:154–174.
26. Crossley AJ, Wright NG. Time accurate local time stepping for the unsteady shallow water equations. *International Journal for Numerical Methods in Fluids* 2005; **48**:775–799.
27. Flaherty R, Loy RM, Shephard MS, Szymanski BK, Teresco JD, Ziantz LH. Adaptive local refinement with octree load-balancing for the parallel solution of three-dimensional conservation laws. *Journal of Parallel and Distributed Computing* 1997; **47**:139–152.
28. Remacle JF, Pinchedez K, Flaherty JE, Shephard MS. An efficient local time stepping discontinuous Galerkin for adaptive transient computations. *Technical Report 2001-13*, SCORECRPI, TROY-NY, 2001.
29. Piperno S. Symplectic local time-stepping in non-dissipative DGTD methods applied to wave propagation problems. *Mathematical Modelling and Numerical Analysis* 2006; **40**:815–841.
30. Dawson CN, Wheeler MF. Time-splitting methods for advection–diffusion–reaction equations arising in contaminant transport. *Proceedings of the Second International Conference on Industrial and Applied Mathematics*, Washington, DC, U.S.A., 1992; 71–82.
31. Lesaint P, Raviart PA. On a finite element method for solving the neutron transport equation. In *Mathematical Aspects of Finite Elements in Partial Differential Equations*, de Boor C (ed.). Academic Press: New York, 1974; 89–145.
32. Chavent G, Cockburn B. The local projection p0–p1 discontinuous-Galerkin finite element method for scalar conservation laws. *Mathematical Modelling and Numerical Analysis* 1989; **23**:565–592.

33. Gowda V, Jaffré J. A discontinuous finite element method for scalar nonlinear conservation laws. *Rapport de Recherche INRIA*, *No. 1848*, 1993.
34. Chavent G, Jaffré J. *Mathematical Models and Finite Elements for Reservoir Simulation*. North Holland: Amsterdam, 1986.
35. Raviart P-A, Thomas J-M. A mixed finite element method for second order elliptic problems. *Mathematical Aspects of Finite Element Method*. Lecture Notes in Mathematics. Springer: New York, 1977; 292–315.
36. Brezzi F, Fortin M. *Mixed and Hybrid Finite Element Methods*. Springer: New York, 1991.
37. Toro E. *Riemann Solvers and Numerical Methods for Fluid dynamics*. Springer: Berlin, 1997.
38. Van Leer B. Towards the ultimate conservative scheme: V. A second order Godunov's method. *Journal of Computational Physics* 1979; **32**:101–136.
39. Hoteit H, Ackerer P, Mosé R, Erhel J, Philippe B. New two-dimensional slope limiters for discontinuous Galerkin methods on arbitrary meshes. *International Journal for Numerical Methods in Engineering* 2004; **61**:2566–2593.
40. Burbeau A, Sagaut P, Bruneau Ch-H. A problem-independent limiter for high-order Runge–Kutta discontinuous Galerkin methods. *Journal of Computational Physics* 2001; **169**:111–150.
41. Bjorck A. *Numerical Methods for Least Squares Problems*. SIAM: Philadelphia, PA, 1996.
42. Chavent G, Roberts JE. A unified physical presentation of mixed, mixed hybrid finite elements and standard finite difference approximations for the determination of velocities in waterflow problems. *Advances in Water Resources* 1991; **14**:329–348.
43. Younes A, Ackerer P, Mosé R, Chavent G. A new formulation of the mixed finite element method for solving elliptic and parabolic PDE with triangular elements. *Journal of Computational Physics* 1999; **149**:148–167.
44. Younes A, Ackerer P, Chavent G. From mixed finite elements to finite volumes for elliptic PDE in 2 and 3 dimensions. *International Journal for Numerical Methods in Engineering* 2004; **59**:365–388.
45. Chavent G, Younes A, Ackerer P. On the finite volume reformulation of the mixed finite element method for elliptic and parabolic PDE on triangles. *Computer Methods in Applied Mechanics and Engineering* 2003; **192**:655–682.
46. Kirby R. On the convergence of high resolution methods with multiple time scales for hyperbolic conservation laws. *Mathematics of Computation* 2002; **72**:1239–1250.
47. Putti M, Yeh W, Mulder W. A triangular finite volume approach with high-resolution upwind terms for the solution of groundwater transport equations. *Water Resources Research* 1990; **26**:2865–2880.
48. Sboui A, Jaffré J. Discrétisation en temps par sous-domaine pour un problème d'advection en milieu poreux. *ARIMA* 2006; **5**:330–346.
49. Sboui A. Quelques méthodes numériques robustes pour l'écoulement et le transport en milieu poreux. *Thèse de Doctorat*, Université Paris Dauphine, 2007.
50. Leij Feike J, Dane JH. Analytical solution of the one-dimensional advection equation and two- or three-dimensional dispersion equation. *Water Resources Research* 1990; **26**:1475–1482.
51. Diersch HJ, Kolditz O. Variable-density flow and transport in porous media: approaches and challenges. *Advances in Water Resources* 2002; **25**:899–944.